Research Article | Vol. 27, No. 26 / 23 December 2019 / Optics Express 37795

Optics EXPRESS

Low loss CMOS-compatible silicon nitride photonics utilizing reactive sputtered thin films

ANDREAS FRIGG,[1,3,4] ANDREAS BOES,[1] GUANGHUI REN,[1] ISLAM ABDO,[1] DUK-YONG CHOI,[2] SILVIO GEES,[3] AND ARNAN MITCHELL[1,5]

[1]School of Engineering, Integrated Photonics and Applications Centre, RMIT University, Melbourne, VIC 3001, Australia
[2]Research School of Physics and Engineering, Australian National University, Canberra, ACT 2601, Australia
[3]Evatec Ltd., Hauptstrasse 1a, 9477 Trübbach, Switzerland
[4]andreas.frigg@evatecnet.com
[5]arnan.mitchell@rmit.edu.au

Abstract: Low temperature deposition of low loss silicon nitride (SiN) thin-films is very attractive as it opens opportunities for realization of multi-layer photonic chips and hybrid integration of optical waveguides with temperature sensitive platforms such as processed CMOS silicon electronics or lithium niobate on insulator. So far, the most common low-temperature deposition technique for SiN is plasma enhanced chemical vapor deposition (PECVD), however such SiN thin-films can suffer from significant losses at C-band wavelengths due to unwanted hydrogen bonds. In this contribution we present a back end of line (< 400°C), low loss SiN platform based on reactive sputtering for telecommunication applications. Waveguide losses of 0.8 dB/cm at 1550 nm and as low as 0.6 dB/cm at 1580 nm have been achieved for moderate confined waveguides which appear to be limited by patterning rather than material. These findings show that reactive sputtered SiN thin-films can have lower optical losses compared to PECVD SiN thin-films, and thus show promise for future hybrid integration platforms for applications such as high Q resonators, optical filters and delay lines for optical signal processing.

1. Introduction

Silicon nitride (SiN) is an attractive material for waveguides in photonic integrated circuits (PICs) as it offers a wide wavelength transparency window from visible (VIS) for biophotonics applications [1–3] to near infrared (NIR) for telecommunication applications [4–6] and out into the mid infrared (MIR) for spectroscopy [7,8]. SiN offers negligible two-photon absorption (β_{TPA}) at 1550 nm and a sufficiently high refractive index (n =~2 at 1550 nm) for tight optical confinement and CMOS-compatible fabrication techniques [9,10]. SiN thin-films for optical waveguides are commonly deposited by either low-pressure chemical vapor deposition (LPCVD) or plasma enhanced chemical vapor deposition (PECVD). LPCVD is a high temperature (> 800°C) process that can produce a high quality, stoichiometric silicon nitride (Si_3N_4) thin-film with low hydrogen bonds after post-annealing at ~1100°C [11], which is ideal for the fabrication of optical waveguides with very low propagation losses. Using LPCVD as a deposition method enables waveguide losses down to 0.1 dB/m [12]. However, the high processing temperatures and the resulting high tensile stress limits the co-integration with sensitive substrates as it is prone to diffusion and crack formation [13]. These limitations mean that LPCVD is usually only applied as a front end of line (FEOL) fabrication process.

The outstanding properties of SiN make it also an attractive material for the back-end-of-line (BEOL) processes, for example the hybrid integration of SiN with silicon on insulator (SOI) [4,14–20], III–V materials [21] and lithium niobate on insulator (LNOI) [22–25]. The hybrid

#380758 https://doi.org/10.1364/OE.380758
Journal © 2019 Received 17 Oct 2019; revised 30 Nov 2019; accepted 6 Dec 2019; published 12 Dec 2019

Optics EXPRESS

integration of SiN (for passive components) on SOI and III–V materials (for active components) can lead to more advanced devices, which require low propagation losses (e.g. optical delay lines) and high power handling capabilities (e.g. frequency combs) [18]. For LNOI the SiN layer can be used to form optically loaded rib waveguide as an alternative to etching the LNOI. This approach offers the advantages of reasonably high index contrast for compact waveguides, low propagation loss and wide transparency window, while also harnessing the mature CMOS-compatible fabrication techniques of SiN [22]. However, for the hybrid integration of SiN with SOI, III–V and LNOI platforms it is important that the processing temperatures stay below ~450°C to mitigate the damaging of active components, temperature sensitive substrates and the resistance of the metal contacts [13].

Plasma enhanced chemical vapor deposition (PECVD) and inductive coupled plasma chemical vapor deposition system (ICP-CVD) are BEOL and low temperature (< 400°C) processes, which can be used to deposit thin-films with low stress. Therefore, these deposition processes overcome some of the limitations that the LPCVD process faces. Nevertheless, it is challenging with PECVD or ICP-CVD to achieve a low concentration of Si-H and N-H bonds, which can introduce unwanted absorption losses at telecommunication wavelengths [26,27]. These bonds limit the waveguides losses typically to 2 dB/cm, which is too high for certain applications such as optical delay lines in microwave photonics signal processing [6] as it prevents long propagation lengths and limits the bandwidth [27–29]. Recently, deuterated silane (SiD_4) precursor have been employed to shift the losses caused by the hydrogen bonds outside of the telecommunication wavelength window. This resulted in reduced waveguides losses of 0.3 dB/cm at C-band wavelengths [29], however the SiD_4 precursor is quite expensive and not readily available, which makes this process less attractive for low-loss waveguide fabrication.

Reactive sputtering is another promising BEOL deposition method for waveguides and might offer lower propagation losses compared to PECVD as it is less likely that H-bonds form during the deposition process [5]. Ultra low loss waveguides in reactive sputtered Ta_2O_5 have been demonstrated in the past for low confinement waveguides [30]. Although there is a high potential for reactive sputtered SiN waveguides a comprehensive study for photonic integrated circuits is missing.

In this contribution, we demonstrate low loss SiN waveguides, which are deposited by reactive sputtering at temperatures below 100°C. We investigate the deposition parameters and their impact on surface roughness, stress and optical losses. SiN thin-films with a surface roughness of R_q of 1.2 nm, stress value of −25 MPa and slab thin-film losses of 1 dB/cm have been achieved. As a post deposition step we investigate thermal annealing at 400° C in ambient atmosphere. We achieved post-annealed slab thin-film losses of approximately 0.25 dB/cm. We also fabricated microring resonators of moderate confined waveguides to demonstrate the viability of this SiN platform. This enabled us to achieve waveguide losses of 1.3 dB/cm ($Q_{int} = 2.68 \times 10^5$) and 0.6 dB/cm ($Q_{int} = 5.81 \times 10^5$) at 1580 nm for single-mode and multi-mode dimensions respectively. Further we evaluated the losses from 1510–1600 nm with worst case waveguide loss of 3.1 dB/cm and 2.1 dB/cm for single-mode and multi-mode dimensions, respectively.

2. Deposition and characterization of silicon nitride thin-films

2.1. SiN thin-films deposition

A commercial reactive magnetron sputtering system (Evatec Clusterline RAD), equipped with DC-pulsed and RF rotating target sources as described in detail in Ref. [31] was used for the deposition of SiN. DC-pulsed sputtering was employed for the SiN deposition with the advantages of a simpler, more stable deposition process with better uniformity and higher rate compared to RF sputtering. The SiN thin-films were grown from a silicon target under Ar/N_2 plasma environment for ~ 50 min at a dynamic rate of 7.5 nm/min (equals to a static rate of 360 nm/min per 4-inch substrate) to achieve a film thickness of 400 nm. As a substrate a 4-inch silicon wafer

Optics EXPRESS

with a 3 µm SiO_2 buried oxide (BOX) layer was used. The wafer temperature stays typically below 100°C during the reactive sputtering process.

We were particularly interested in optimizing the process parameter such as Ar/N_2 ratio, pressure, DC-power and DC pulse settings in order to achieve stoichiometric low optical loss, low stress, low roughness and highly uniform SiN thin-films.

Figure 1(a) shows the influence of the Ar/N_2 ratio on the refractive index, which was measured using an ellipsometer (Woollam M2000 and Sentech SE 800-PV). When increasing the Ar/N_2 ratio the thin-film composition can be adjusted from N-rich to stoichiometric and Si-rich SiN. Our aim was a near-stoichiometric SiN thin-film, which was achieved with an Ar/N_2 ratio of 1.5 resulting in a refractive index n = 2.02 (± 0.01) at 633 nm. These results are in good agreement with the findings of Mousinho et al. [32]. A rate increase of 75% was observed when increasing the Ar/N_2 ratio from 0.25 to 2.3. The near-stoichiometric SiN thin-films also yielded the lowest optical losses and stress when compared to N-rich or Si-rich samples.

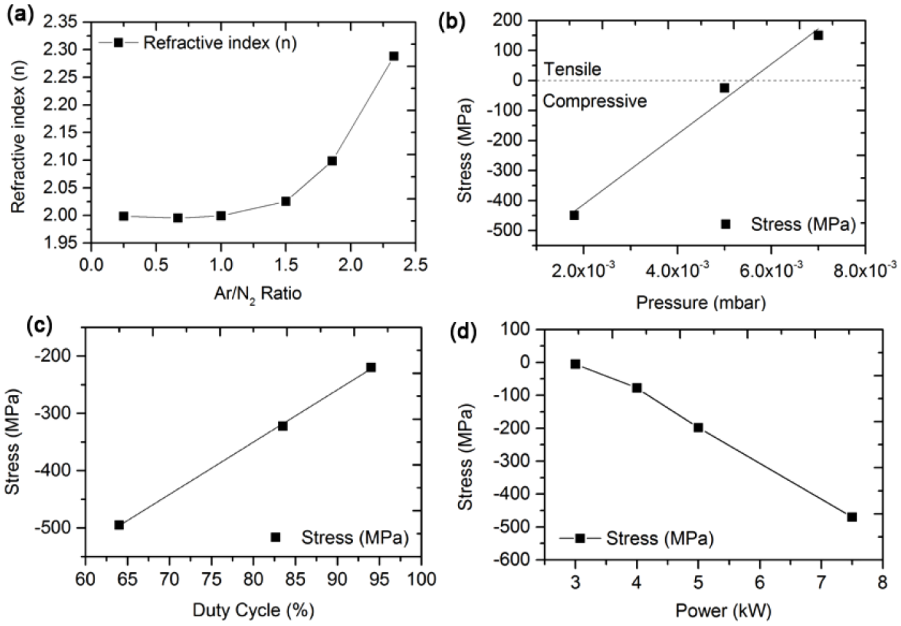

Fig. 1. (a) Refractive index for Ar/N_2 ratios from 0.25 to 2.3; (b) Stress versus chamber pressure; (c) Stress versus DC-pulsed duty cycle; (d) Stress versus DC-pulse power.

Another limiting factor is the stress, which can lead to the cracks or delamination off the deposited SiN. This has been a main point of concern in LPCVD SiN thin-films, where high tensile stress limits the maximum deposition thickness (~400–700 nm) without applying additional process steps such as trenches or the damascene process [33,34]. With reactive sputtering film thicknesses up to 8 µm without cracks where previously demonstrated [35]. Film stress measurements were carried out using a laser based measurement tool (Tencor FLX-2320) for pre and post-deposition measurement of the wafer bow. By increasing the deposition chamber pressure it was possible to reverse the −450 MPa compressive stress level into + 150 MPa tensile, while keeping all other parameters constant (Fig. 1(b)). This can be explained by a decrease in film density when depositing at higher pressures, following the reactive sputtering structural diagram by Thornton [36] and confirms the findings of Mescher et al. [37] and Schmidt et al. [35]. A decrease of 25% in deposition rate was observed when depositing at higher pressures of 8.0×10^{-3} mbar compared to 2.0×10^{-3} mbar. Figure 1(c) shows the influence of the DC-pulsed duty cycle on the thin-film stress. The duty cycle was changed by modifying the pulse off time

Optics EXPRESS

between 0.4 µs to 2.4 µs. All other deposition parameters were kept constant. Increasing the duty cycle reduces the stress level significantly from −500 MPa to −200 MPa due to the lower pulse power density when running at higher duty cycles. Figure 1(d) shows the influence on DC-power on the thin-film stress. It was found that the stress becomes more compressive when increasing the DC-power (resulting in an increasing deposition rate). Both of these findings are in good agreement with the studies of Schmidt et al. [35] and Chason et al. [38].

For the final deposition run we used an optimized chamber pressure of 5.0×10^{-3} mbar, DC-pulse power of 3 kW and DC-pulse duty cycle of 88% as the best trade-off between stress (−25 MPa), roughness ($R_q = 1.2$ nm) and bulk material loss (0.25 dB/cm).

2.2. SiN thin-films characterization

In order to investigate the effect of hydrogen bonds on material loss for deposited SiN thin-film, Fourier transform infrared spectroscopy FTIR (Perkin Elmer, Spectrum two) was used to analyze the IR-absorption losses. The resulting spectrum is shown in Fig. 2(a). One can see that the reactive sputtered SiN thin-films do not exhibit Si-H (~ 2160 cm^{-1}) or N-H Bond (~3340 cm^{-1}) absorption peaks in the IR spectra. This observation can be explained by the fact that that the reactive sputtering process only uses N_2 as a reactant gas, which is in contrast to the PECVD deposition processes, where a $SiH_4/NH_3/N_2$ chemistry is used. These findings are in accordance with the results by Zhang et al. [5].

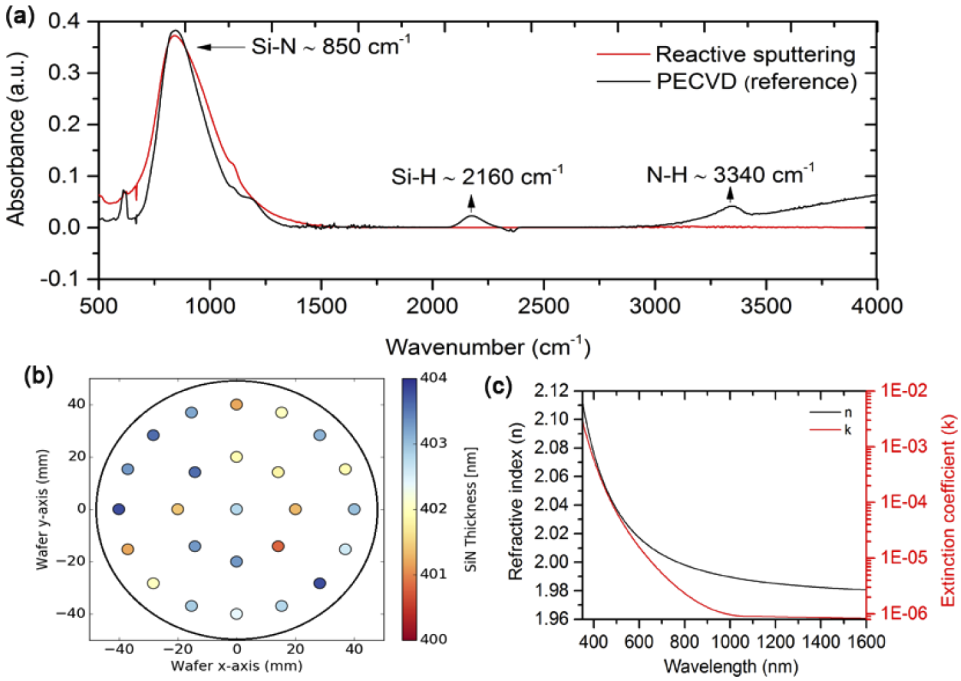

Fig. 2. (a) FTIR absorption spectra of reactive sputtered SiN indicating no Si-H and N-H bond losses compare to a PECVD reference; (b) Thickness uniformity of ± 0.5% measured on a 4-inch wafer; (c) Dispersion and extinction profile for reactive sputtered SiN with absorption optimized Ar/N_2 ratio.

Afterwards, we analyzed the thickness uniformity and dispersion, which is important to achieve consistent waveguide dimensions over large substrate areas when fabricating photonic devices. Figure 2(b) shows a thickness uniformity of ± 0.5% measured across a 4 inch wafer, which can be optimized further by adjusting the Si-target to substrate distance [39]. Figure 2(c) shows the

Optics EXPRESS

dispersion and extinction coefficient over a wide wavelength range from 400–1600 nm for an optimized Ar/N_2 ratio of 1.5.

Next, we analyzed the surface roughness as a thin-film with a low surface roughness is beneficial to reduce light scattering from the surface and grain boundaries [11,12]. The surface roughness of the SiN thin-films was investigated by using an atomic force microscopy (Park System, NX20). We measured an rms roughness of $R_q = 1.2$ nm (see Figs. 3(a) and 3(b)). This value is lower than comparable PECVD SiN thin-films, which are typically in the order of $R_q \sim 2$ nm [27]. The surface roughness can further be reduced by using chemical mechanical polishing (CMP) [12].

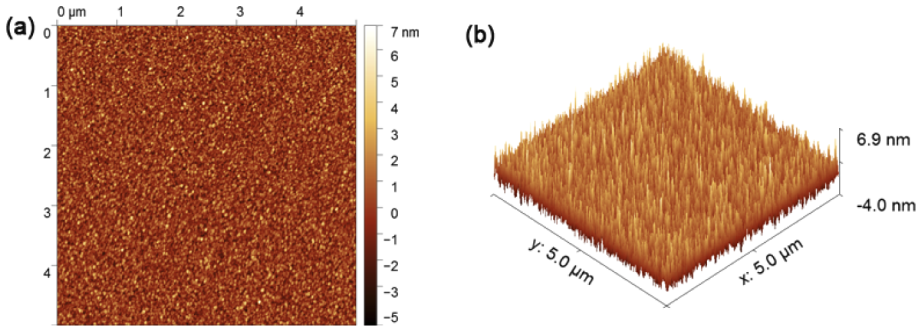

Fig. 3. (a) 2D-plot of SiN roughness measured by atomic force microscope over an area of 5×5 µm; (b) 3D-plot of the sputtered SiN surface.

Then we characterized the slab material loss using a prism coupler measurement [40] (Metricon 2010M) to confirm the viability of our reactive sputtered SiN thin-films for photonic integrated circuits prior to the waveguide fabrication. The loss was determined by coupling a 1550 nm laser into the SiN thin-film and analyzing the decay of the scattered light at the surface of the SiN thin-film as it propagates along the sample. The propagation losses of the reactive sputtered SiN at 1550 nm were 1 dB/cm as-deposited and 0.25 dB/cm with a post-annealing step at 400°C. This shows that a post annealing step is beneficial to reduce the optical losses in the sputtered SiN thin-films, which could originate from uncompleted bond structures due to dynamic sputtering process at room temperature or residual hydrogen in the sputtering chamber. Further evaluation is needed to confirm the post-annealing related structural changes of the thin-film. The annealing temperature is well below the SiN crystallization temperature of 1200°C [41] and therefore does not change the amorphous structure of the thin-film. The moderate temperatures of the post-annealing are similar to the temperatures in standard PECVD processes and therefore can still be employed as a BEOL fabrication process.

3. Waveguide losses of the reactive sputtered silicon nitride thin-films

In this work we investigated moderate confined waveguides with a cross-section of 1.0 µm × 0.4 µm (width × height) and 2.0 µm × 0.4 µm for single-mode and multi-mode waveguides, respectively. The following subsections outline the fabrication of microring resonator for waveguide loss measurements through analyzing the quality factor of the resonances.

3.1. Fabrication of microring resonator

All-pass microring resonators with different radii (30, 60, 90 and 120 µm) were fabricated using the thin films described in Section 2. ZEP 520A positive resist was used for the pattering of the microring resonators with a Vistec EBPG5000 electron-beam lithography (EBL) system (100 kV). A resist post exposure bake for 5 minutes at 100°C was employed to improve the selectivity and

Optics EXPRESS

reduce the etching induced roughness. The SiN was fully etched using inductive coupled plasma (ICP) etching (Oxford Instrument Plasmalab 100) as evident by the SEM cross-section of a 1 µm wide SiN waveguide shown in Fig. 4(c). Figures 4(a) and 4(b) show the fundamental TE mode for the single-mode and multi-mode waveguides, respectively. The etching recipe with a mixture of CHF_3 and O_2 was optimized to achieve vertical and smooth sidewalls (Fig. 4(d)). Afterwards, the waveguides were cladded using 3 µm SiO_2 deposited by PECVD (Oxford Instrument Plasmalab 100). Figure 4(e) shows an optical microscopy image of the fabricated microring resonator. Sub-micron inverse tapers with average coupling losses of 3 dB per facet were used to couple light in and out of the waveguide, which was interfaced with lensed fibers.

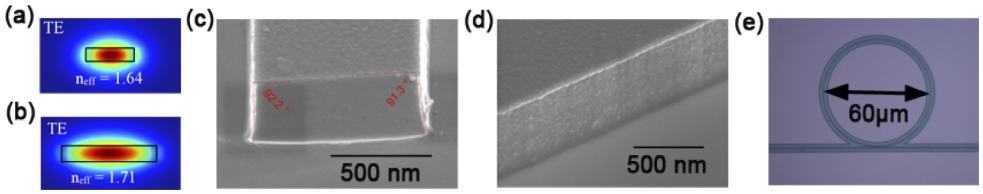

Fig. 4. (a) TE-Mode profile with a cross-section of 1.0 × 0.4 µm, (b) TE-Mode profile with a cross-section of 2.0 × 0.4 µm; (c) SEM image of the waveguide cross section 1.0 × 0.4 µm; (d) SEM image of the etched waveguide indicating a low sidewall roughness; (e) Fabricated ring resonator with 30 µm ring radius. The ring resonator is coupled to a straight waveguide of the same dimensions.

3.2. Measurement of microring resonator

The spectral responses of the micro ring resonators were characterized using a tunable laser source (Agilent 8164A), with the resolution of 0.1 pm. The laser was connected to a polarization maintaining fiber, coupling TE-polarized light into the fabricated chip through the inverse tapers with a tip width of 300 nm. The chip was mounted on a precision translation stage. Figure 5(a) presents the spectral response for a single mode microring with a radius of 90 µm. One can see periodic and sharp resonances, which are caused by fundamental TE-mode of the ring resonator with a measured free spectral range (FSR) of 2.14 nm as well as a sinusoidal wavelength response, which is caused by Fabry-Perot oscillations corresponding to the superimposed waveguide facet reflections. Beside small resonances, which might correspond to remaining TM polarization, are visible. The measured free spectral range (FSR) for this resonator is 2.14 nm and the full width half maximum (FWHM) of the resonance is $\delta\lambda = 9.1$ pm, which corresponds to loaded quality factor (Q_{loaded}) of 1.71×10^5 at $\lambda_0 = 1553$ nm (Fig. 5(a), insert). The resonator is slightly under-coupled at this wavelength. The intrinsic quality factor Q_{int} of the resonator can be calculated by [42]

$$Q_{\text{int}} = \frac{2Q_{\text{loaded}}}{1 + \sqrt{T_o}} \tag{1}$$

where T_0 is the fraction of transmitted optical power at the resonant wavelength λ_0. With the measured $T_0 = 0.21$ we calculated an intrinsic quality factor $Q_{\text{int}} = 2.33\times 10^5$ using Eq. (1). We also analyzed the resonances for a multi-mode waveguide microring resonator with the same radius and calculated an intrinsic quality factor of 4.18×10^5 at 1548 nm (Fig. 5(b)) and 5.81×10^5 at 1579 nm (Fig. 5(c)), respectively. The fundamental TE-mode FSR for the multi-mode waveguide is 2.12 nm.

To investigate the wavelength dependent propagation losses, the resonances were measured from 1510 nm to 1600 nm. The propagation losses and group index n_g were calculated using the

Optics EXPRESS

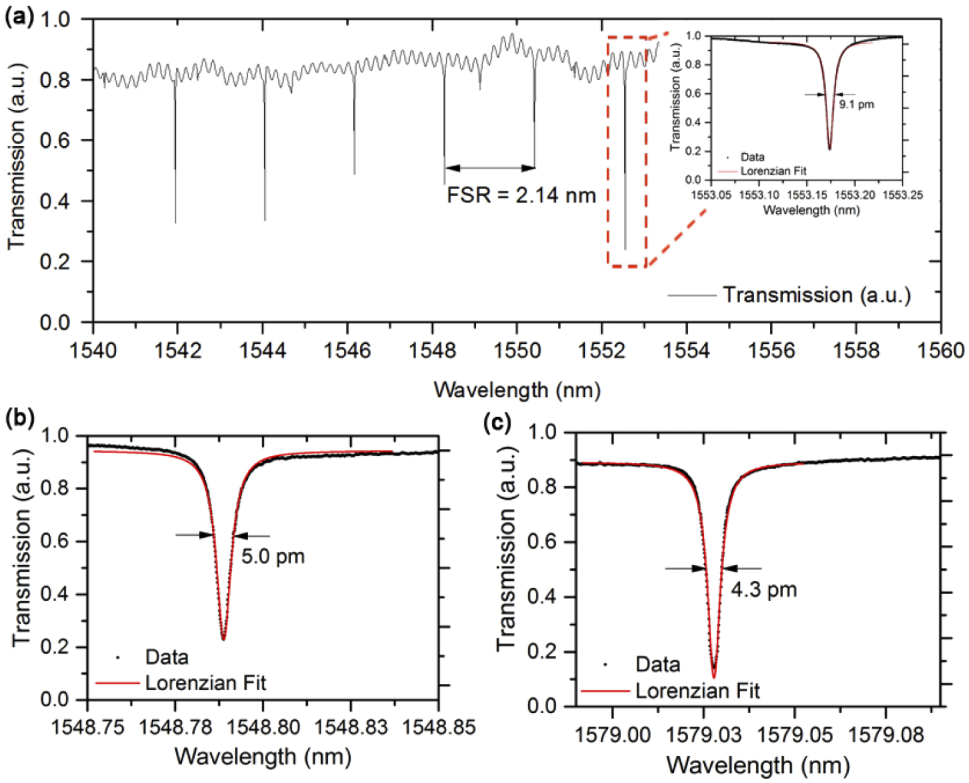

Fig. 5. (a) Measured transmission spectrum of the single-mode waveguide microring resonator with an FSR = 2.14 nm and an insert of a single resonance at 1553 nm with an intrinsic quality factor (Q_{int}) of 2.33×10^5; (b) A measured resonance at 1548 nm for a multi-mode waveguide microring resonators with an intrinsic quality factor (Q_{int}) of 4.18×10^5; (c) A measured resonance at 1579 nm for a multi-mode waveguide microring resonators with an intrinsic quality factor (Q_{int}) of 5.81×10^5.

following equation [42]

$$\alpha = \frac{2\pi n_g}{Q_{\text{int}}\lambda_0} = \frac{\lambda_0}{Q_{\text{int}} \times R \times FSR} \tag{2}$$

where n_g is the group index, λ_0 is the resonant wavelength, Q_{int} is the intrinsic quality factor, R is the radius and FSR is the free spectral range of the microring resonator.

We calculated a group index n_g of 1.93 and 2.00 for single-mode and multi-mode dimensions, respectively. The lower quality factor of the single-mode waveguide resonator (Fig. 5(a), insert) compared to the multi-mode waveguide resonator (Fig. 5(b)) at 1550 nm indicates that the waveguide losses of the single mode waveguides are strongly influenced by the mode overlap with the waveguide sidewalls (Figs. 4(a) and 4(b)), where etching induced roughness causes scattering [11]. We believe that these waveguide losses could be further improved by applying multipass EBL lithography and further optimizing the etching recipe [12]. With these improvements the waveguide losses should approach the 0.25 dB/cm levels measured for the unprocessed films. Figure 6(a) and Fig. 6(b) show the waveguide losses and intrinsic quality factor for single-mode and multi-mode microring resonators, respectively. Worst case propagation losses of 3.1 dB/cm for single-mode (Fig. 6(a)) and 2.1 dB/cm for multi-mode (Fig. 6(b)) microring resonators have been observed in the wavelength range of 1510–1600 nm.

Optics EXPRESS

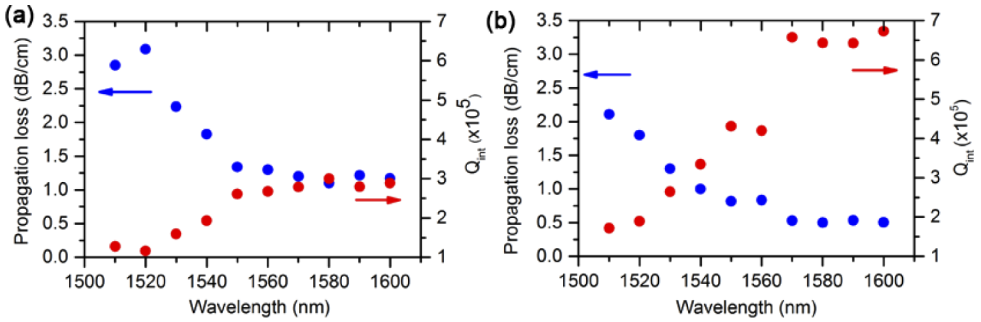

Fig. 6. (a) Propagation losses and intrinsic quality factor in the wavelength range of 1510–1600 nm for a single-mode microring resonator with a ring radius of 90 µm; (b) Propagation losses and intrinsic quality factor for multi-mode microring resonator with a ring radius of 90 µm.

When comparing the multi-mode microring resonator losses of 0.62 dB/cm from 1550–1600 nm with the losses of 1.4 dB/cm from 1510–1550 nm (where the Si-H bonds have a vibrational overtone at ~ 1520 nm) one can see that the losses increase ~ 0.8 dB/cm (Fig. 5(b)). Further investigation is needed to evaluate the origin of these losses, which could be caused by the SiN core or PECVD SiO_2 cladding layer.

In Table 1 we compared our results to state of the art SiN platforms for moderate confined waveguides for different SiN deposition methods. With reactive sputtering, waveguide losses below previously reported values for low temperature SiN have been achieved from 1510–1600 nm. A major advantage of reactive sputtering compared to PECVD are the low H-bond related losses in reactive sputtered SiN allowing us to achieve considerably low losses (< 3 dB/cm) from 1510–1550 nm compared to values of > 8 dB/cm in PECVD [4,14,17,28]. These losses compare well to the high temperature LPCVD deposited Si_3N_4 counterparts with similar cross-sections prior to post-annealing at ~1100°C [14,17,44]. However, it should be noted that we believe that

Table 1. Summary of propagation losses for state of the art SiN waveguides deposited by PECVD, ICP-CVD and LPCVD compared with reactive sputtering.

Dimension (µm × µm) width × height	Deposition technology and temperature	Wavelength [nm]	Propagation loss (dB/cm)	Reference
0.7 × 0.4	PECVD ~350°C	1550	2.1 ± 0.2	[27]
1.0 × 0.4	PECVD ~350°C	1550 / 1580	3.0 / 1.0	[4]
1.0 × 0.6	PECVD ~350°C	1550 /1580	3.5 / 0.8	[17]
1.0 × 0.4	PECVD ~350°C	1550 / 1580	3.75 / 1.1	[17]
1.4 × 0.6	ICP-CVD 75°C	1500–1545 / 1550–1600	>10 / 0.79	[28]
1.2 × 0.58	PECVD ~350°C	1550 /1600	4.99 / 2.63	[43]
1.2 × 0.58	PECVD + Annealing 1150°C	1550 /1600	1.27 / 1.08	[43]
1.0 × 0.4	LPCVD 800°C	1550 / 1580	1.3 / 0.4	[17]
1.0 × 0.4	LPCVD 700°C	1550	0.72	[44]
1.0 × 0.4	**Reactive sputtering + Annealing 400°C**	**1550 / 1580**	**1.5 /1.1**	**[This work]**
2.0 × 0.4	**Reactive sputtering + Annealing 400°C**	**1550 / 1580**	**0.8 / 0.6**	**[This work]**

Optics EXPRESS

the losses are currently limited by scattering from the sidewall roughness rather than H-bond absorption losses.

4. Conclusion

We have investigated and optimized the SiN deposition by reactive sputtering at low temperatures for photonic integrated circuits. SiN thin-film losses of 0.25 dB/cm have been achieved with a low stress value of −25 MPa at a maximum processing temperature of 400°C. Microring resonators have been fabricated to show the viability of SiN thin-films for integrated photonic circuits (PICs). With the sputtered SiN thin-films, we were able to demonstrate waveguides with loss of 0.8 and of 0.6 dB/cm at 1550 nm and 1580 nm, respectively. A comparison of single mode and multi-mode waveguides suggested these values are currently limited by scattering from sidewall roughness. Further we evaluated the waveguide losses across a wide wavelength range from 1510–1600 nm to investigate the Si-H related loss, which has a much lower vibrational overtone centered at ~ 1520 nm compared with PECVD SiN. Therefore SiN based on reactive sputtering opens up new perspective for straight forward fabrication and integration of low loss waveguides into BEOL processes and temperature sensitive substrates.

Funding

Australian Research Council (DP190101576, DP190102773).

Acknowledgments

The authors acknowledge the facilities, and the scientific and technical assistance, of the Micro Nano Research Facility (MNRF) and the Australian Microscopy & Microanalysis Research Facility at RMIT University. This work was performed in part at the Melbourne Centre for Nanofabrication (MCN) in the Victorian Node of the Australian National Fabrication Facility (ANFF).

Disclosures

The authors declare no conflicts of interest. AG, SG:Evatec Ltd (E, F)

References

1. M. C. Estevez, M. Alvarez, and L. M. Lechuga, "Integrated optical devices for lab-on-a-chip biosensing applications," Laser Photonics Rev. **6**(4), 463–487 (2012).
2. A. Subramanian, P. Neutens, A. Dhakal, R. Jansen, T. Claes, X. Rottenberg, F. Peyskens, S. Selvaraja, P. Helin, and B. Du Bois, "Low-loss singlemode PECVD silicon nitride photonic wire waveguides for 532–900 nm wavelength window fabricated within a CMOS pilot line," IEEE Photonics J. **5**(6), 2202809 (2013).
3. A. Gorin, A. Jaouad, E. Grondin, V. Aimez, and P. Charette, "Fabrication of silicon nitride waveguides for visible-light using PECVD: a study of the effect of plasma frequency on optical properties," Opt. Express **16**(18), 13509–13516 (2008).
4. N. Sherwood-Droz and M. Lipson, "Scalable 3D dense integration of photonics on bulk silicon," Opt. Express **19**(18), 17758–17765 (2011).
5. Z. Zhang, M. Yako, K. Ju, N. Kawai, P. Chaisakul, T. Tsuchizawa, M. Hikita, K. Yamada, Y. Ishikawa, and K. Wada, "A new material platform of Si photonics for implementing architecture of dense wavelength division multiplexing on Si bulk wafer," Sci. Technol. Adv. Mater. **18**(1), 283–293 (2017).
6. L. Zhuang, D. Marpaung, M. Burla, W. Beeker, A. Leinse, and C. Roeloffzen, "Low-loss, high-index-contrast Si3N4/SiO2 optical waveguides for optical delay lines in microwave photonics signal processing," Opt. Express **19**(23), 23162–23170 (2011).
7. H. Guo, C. Herkommer, A. Billat, D. Grassani, C. Zhang, M. H. P. Pfeiffer, W. Weng, C.-S. Brès, and T. J. Kippenberg, "Mid-infrared frequency comb via coherent dispersive wave generation in silicon nitride nanophotonic waveguides," Nat. Photonics **12**(6), 330–335 (2018).
8. A. Dutt, C. Joshi, X. Ji, J. Cardenas, Y. Okawachi, K. Luke, A. L. Gaeta, and M. Lipson, "On-chip dual-comb source for spectroscopy," Sci. Adv. **4**(3), e1701858 (2018).

Optics EXPRESS

9. A. Rahim, E. Ryckeboer, A. Z. Subramanian, S. Clemmen, B. Kuyken, A. Dhakal, A. Raza, A. Hermans, M. Muneeb, S. Dhoore, Y. Li, U. Dave, P. Bienstman, N. L. Thomas, G. Roelkens, D. V. Thourhout, P. Helin, S. Severi, X. Rottenberg, and R. Baets, "Expanding the Silicon Photonics Portfolio With Silicon Nitride Photonic Integrated Circuits," J. Lightwave Technol. **35**(4), 639–649 (2017).
10. A. E. Kaloyeros, F. A. Jové, J. Goff, and B. Arkles, "Review—Silicon Nitride and Silicon Nitride-Rich Thin Film Technologies: Trends in Deposition Techniques and Related Applications," ECS J. Solid State Sci. Technol. **6**(10), P691–P714 (2017).
11. M. J. Shaw, J. Guo, G. A. Vawter, S. Habermehl, and C. T. Sullivan, *Fabrication techniques for low-loss silicon nitride waveguides, MOEMS-MEMS Micro and Nanofabrication* (SPIE, 2005), Vol. 5720.
12. X. Ji, F. A. S. Barbosa, S. P. Roberts, A. Dutt, J. Cardenas, Y. Okawachi, A. Bryant, A. L. Gaeta, and M. Lipson, "Ultra-low-loss on-chip resonators with sub-milliwatt parametric oscillation threshold," Optica **4**(6), 619–624 (2017).
13. Y. H. D. Lee and M. Lipson, "Back-End Deposited Silicon Photonics for Monolithic Integration on CMOS," IEEE J. Sel. Top. Quantum Electron. **19**(2), 8200207 (2013).
14. W. D. Sacher, Y. Huang, G. Lo, and J. K. S. Poon, "Multilayer Silicon Nitride-on-Silicon Integrated Photonic Platforms and Devices," J. Lightwave Technol. **33**(4), 901–910 (2015).
15. W. D. Sacher, J. C. Mikkelsen, Y. Huang, J. C. C. Mak, Z. Yong, X. Luo, Y. Li, P. Dumais, J. Jiang, D. Goodwill, E. Bernier, P. G. Lo, and J. K. S. Poon, "Monolithically Integrated Multilayer Silicon Nitride-on-Silicon Waveguide Platforms for 3-D Photonic Circuits and Devices," Proc. IEEE **106**(12), 2232–2245 (2018).
16. Q. Wilmart, D. Fowler, C. Sciancalepore, K. Hassan, S. Plantier, L. Adelmini, S. Garcia, D. Robin-Brosse, S. Malhouitre, and S. Olivier, *A hybrid SOI/SiN photonic platform for high-speed and temperature-insensitive CWDM optical transceivers, SPIE OPTO* (SPIE, 2018), Vol. 10537.
17. Y. Huang, J. Song, X. Luo, T.-Y. Liow, and G.-Q. Lo, "CMOS compatible monolithic multi-layer Si3N4-on-SOI platform for low-loss high performance silicon photonics dense integration," Opt. Express **22**(18), 21859–21865 (2014).
18. Q. Li, A. A. Eftekhar, M. Sodagar, Z. Xia, A. H. Atabaki, and A. Adibi, "Vertical integration of high-Q silicon nitride microresonators into silicon-on-insulator platform," Opt. Express **21**(15), 18236–18248 (2013).
19. J. F. Bauters, M. L. Davenport, M. J. R. Heck, J. K. Doylend, A. Chen, A. W. Fang, and J. E. Bowers, "Silicon on ultra-low-loss waveguide photonic integration platform," Opt. Express **21**(1), 544–555 (2013).
20. Q. Wilmart, H. El Dirani, N. Tyler, D. Fowler, S. Malhouitre, S. Garcia, M. Casale, S. Kerdiles, K. Hassan, C. Monat, X. Letartre, A. Kamel, M. Pu, K. Yvind, L. K. Oxenløwe, W. Rabaud, C. Sciancalepore, B. Szelag, and S. Olivier, "A Versatile Silicon-Silicon Nitride Photonics Platform for Enhanced Functionalities and Applications," Appl. Sci. **9**(2), 255 (2019).
21. M. Piels, J. F. Bauters, M. L. Davenport, M. J. R. Heck, and J. E. Bowers, "Low-Loss Silicon Nitride AWG Demultiplexer Heterogeneously Integrated With Hybrid III–V/Silicon Photodetectors," J. Lightwave Technol. **32**(4), 817–823 (2014).
22. A. Boes, L. Chang, M. Knoerzer, T. G. Nguyen, J. D. Peters, J. E. Bowers, and A. Mitchell, "Improved second harmonic performance in periodically poled LNOI waveguides through engineering of lateral leakage," Opt. Express **27**(17), 23919–23928 (2019).
23. L. Chang, M. H. P. Pfeiffer, N. Volet, M. Zervas, J. D. Peters, C. L. Manganelli, E. J. Stanton, Y. Li, T. J. Kippenberg, and J. E. Bowers, "Heterogeneous integration of lithium niobate and silicon nitride waveguides for wafer-scale photonic integrated circuits on silicon," Opt. Lett. **42**(4), 803–806 (2017).
24. A. N. R. Ahmed, S. Shi, M. Zablocki, P. Yao, and D. W. Prather, "Tunable hybrid silicon nitride and thin-film lithium niobate electro-optic microresonator," Opt. Lett. **44**(3), 618–621 (2019).
25. A. Honardoost, F. A. Juneghani, R. Safian, and S. Fathpour, "Towards subterahertz bandwidth ultracompact lithium niobate electrooptic modulators," Opt. Express **27**(5), 6495–6501 (2019).
26. E. A. Douglas, P. Mahony, A. Starbuck, A. Pomerene, D. C. Trotter, and C. T. DeRose, "Effect of precursors on propagation loss for plasma-enhanced chemical vapor deposition of SiNx:H waveguides," Opt. Mater. Express **6**(9), 2892–2903 (2016).
27. S. Mao, S. Tao, Y. Xu, X. Sun, M. Yu, G. Lo, and D. Kwong, "Low propagation loss SiN optical waveguide prepared by optimal low-hydrogen module," Opt. Express **16**(25), 20809–20816 (2008).
28. Z. Shao, Y. Chen, H. Chen, Y. Zhang, F. Zhang, J. Jian, Z. Fan, L. Liu, C. Yang, L. Zhou, and S. Yu, "Ultra-low temperature silicon nitride photonic integration platform," Opt. Express **24**(3), 1865–1872 (2016).
29. T. Hiraki, T. Aihara, H. Nishi, and T. Tsuchizawa, "Deuterated SiN/SiON Waveguides on Si Platform and Their Application to C-Band WDM Filters," IEEE Photonics J. **9**(5), 1–7 (2017).
30. M. Belt, M. L. Davenport, J. E. Bowers, and D. J. Blumenthal, "Ultra-low-loss Ta2O5-core/SiO2-clad planar waveguides on Si substrates," Optica **4**(5), 532–536 (2017).
31. S. Schwyn Thöny, M. Chesaux, S. Gees, and A. Frigg, "Innovative Sputter System for High Volume Production of Demanding Optical Interference Coatings," in *Optical Interference Coatings 2016, OSA Technical Digest (online)* (Optical Society of America, 2016), WA.7.
32. A. P. Mousinho, R. Mansano, L. Zambom, and A. Passaro, *Low temperature deposition of low stress silicon nitride by reactive magnetron sputtering* (2012), Vol. 370.
33. K. Luke, A. Dutt, C. B. Poitras, and M. Lipson, "Overcoming Si3N4 film stress limitations for high quality factor ring resonators," Opt. Express **21**(19), 22829–22833 (2013).

Optics EXPRESS

34. M. H. P. Pfeiffer, C. Herkommer, J. Liu, T. Morais, M. Zervas, M. Geiselmann, and T. J. Kippenberg, "Photonic Damascene Process for Low-Loss, High-Confinement Silicon Nitride Waveguides," IEEE J. Sel. Top. Quantum Electron. **24**(4), 1–11 (2018).
35. S. Schmidt, T. Hänninen, J. Wissting, L. Hultman, N. Goebbels, A. Santana, M. Tobler, and H. Högberg, "SiNx coatings deposited by reactive high power impulse magnetron sputtering: Process parameters influencing the residual coating stress," J. Appl. Phys. **121**(17), 171904 (2017).
36. J. A. Thornton, "Influence of apparatus geometry and deposition conditions on the structure and topography of thick sputtered coatings," J. Vac. Sci. Technol. **11**(4), 666–670 (1974).
37. M. J. Mescher, M. L. Reed, and T. E. Schlesinger, "Stress Control in Sputtered Silicon Nitride Films," Mater. Res. Soc. Symp. Proc. **472**, 239 (1997).
38. E. Chason, M. Karlson, J. J. Colin, D. Magnfält, K. Sarakinos, and G. Abadias, "A kinetic model for stress generation in thin films grown from energetic vapor fluxes," J. Appl. Phys. **119**(14), 145307 (2016).
39. M. Chesaux, S. S. Thöny, S. Gees, and A. Frigg, "Rotating Target Source: Novel Shaperless Concept for Magnetron Sputtering with Excellent Uniformity," in *Optical Interference Coatings 2016, OSA Technical Digest (online)* (Optical Society of America, 2016), WA.2.
40. X. C. Tong, *Advanced Materials for Integrated Optical Waveguides* (Springer, 2014).
41. R. Riedel and M. Seher, "Crystallization behaviour of amorphous silicon nitride," J. Eur. Ceram. Soc. **7**(1), 21–25 (1991).
42. L.-W. Luo, G. S. Wiederhecker, J. Cardenas, C. Poitras, and M. Lipson, "High quality factor etchless silicon photonic ring resonators," Opt. Express **19**(7), 6284–6289 (2011).
43. L. Wang, W. Xie, D. Van Thourhout, Y. Zhang, H. Yu, and S. Wang, "Nonlinear silicon nitride waveguides based on a PECVD deposition platform," Opt. Express **26**(8), 9645–9654 (2018).
44. H. Zhang, C. Li, X. Tu, J. Song, H. Zhou, X. Luo, Y. Huang, M. Yu, and G. Q. Lo, "Efficient silicon nitride grating coupler with distributed Bragg reflectors," Opt. Express **22**(18), 21800–21805 (2014).